

UCRL-8878  
Pg 3.

UNIVERSITY OF  
CALIFORNIA  
*Ernest O. Lawrence*  
*Radiation*  
*Laboratory*

For Reference

Not to be taken from this room

BERKELEY, CALIFORNIA

For Int. Conference on High Energy Accelerators  
and Inst. Geneva Sept. 14-11

UCRL-8878

UNIVERSITY OF CALIFORNIA  
Lawrence Radiation Laboratory  
Berkeley, California

Contract No. W-7405-eng-48

A SEPARATED 1.17-Bev/c  $K^-$  MESON BEAM  
Phillippe Eberhard, Myron L. Good, and Harold K. Ticho

August 25, 1959

A SEPARATED 1.17-Bev/c  $K^-$  MESON BEAM

Phillippe Eberhard, Myron L. Good, and Harold K. Ticho

Lawrence Radiation Laboratory  
University of California  
Berkeley, California

August 25, 1959

Abstract

This report describes the design and testing of a 1.17-Bev/c separated  $K^-$  beam designed in the fall of 1958 in connection with a 15-in. hydrogen bubble chamber experiment. At the target the  $K^-/\pi^-$  ratio was 1/140. At the chamber, after two stages of electromagnetic separation and 4.0  $K^-$ -meson decay lengths, the  $K^-/\pi^-$  ratio was 12.5, corresponding to a total pion suppression by a factor of about  $10^5$ . The  $K^-$  flux at the chamber was 0.87  $K^-$  per  $10^{10}$  protons on the target.

A SEPARATED 1.17-Bev/c  $K^-$  MESON BEAM  
Phillippe Eberhard, Myron L. Good, and Harold K. Ticho \*

Lawrence Radiation Laboratory  
University of California  
Berkeley, California

August 25, 1959

Introduction

During the fall of 1958 a beam of negative K mesons of  $\sim 1.2$  Bev/c momentum was required at the Lawrence Radiation Laboratory in connection with an experiment involving the 15-in. hydrogen bubble chamber. In counting experiments it is possible to distinguish the K mesons from the much more copious pion flux by time-of-flight and Cerenkov counter techniques. Such techniques could also be used for bubble chamber research, especially when coupled with hodoscopic identification of the K mesons in the chamber. However,  $\sim 30$  beam tracks per picture is the maximum that can be handled with good scanning and analyzing efficiency; on the other hand, with the presently available beam levels in the Bevatron ( $2 \times 10^{11}$  protons per pulse) and existing focusing equipment (8-in. -diameter quadrupole strong-focusing lenses) some 300  $K^-$  mesons could be guided from target to chamber on each pulse. Under these circumstances it becomes highly advantageous to increase the target-to-chamber distance so that, while a large fraction of the K mesons decay in flight, the intervening space may be used to effect a spatial separation of the K mesons from the pion background. A beam of this character is described in the following report.

In view of the fact that the momentum dispersion of beams from the Bevatron imposes symmetry about the median plane only, it seemed desirable to adopt a separation scheme in which the pions to be rejected would be deflected out of the median plane. A velocity spectrometer with a horizontal magnetic field H and a vertical electric field E has such a character. Such spectrometers, with deflection plates 230 in. long and capable of supporting  $\sim 400$  kv, had recently become available at the laboratory for enriching antiproton beams.<sup>1</sup> When a momentum-analyzed beam of particles of various masses is shot into such a

---

\*Permanent address: Physics Department, University of California, Los Angeles.

<sup>1</sup>Coombes, Cork, Galbraith, Lambertson, and Wenzel, Phys. Rev. 112, 1303 (1958).

spectrometer, particles with velocity

$$\beta_0 = \frac{E}{H} \quad (1)$$

continue undeflected while others suffer deflections  $\alpha$  out of the median plane:

$$\alpha = \frac{P_0}{P} \Delta \left( \frac{1}{\beta} \right), \quad (2a)$$

$$P_0 = V \frac{\ell}{d}, \quad (2b)$$

where  $P$  is the particle momentum in  $ev/c$ ,  $V$  is the potential applied to the plates in volts,  $\ell$  and  $d$  are the length and separation of the plates, respectively, and  $\Delta(1/\beta)$  is the deviation of  $(1/\beta)$  of the particle from  $1/\beta_0$ . In the relativistic domain ( $p/\mu \gg 1$ ),

$$\frac{\alpha}{P_0} \approx \frac{\mu_1^2 - \mu_0^2}{2P^3}, \quad (3)$$

where  $\mu_0$  is the mass of the particle to which Eq. (1) applies and  $\mu_1$  is the mass of the particle to be deflected. In Fig. 1, the angle  $\alpha_\pi$  of pions relative to K mesons and angle  $\alpha_p$  of protons relative to K mesons are plotted as functions of momentum. A very desirable feature of the velocity spectrometer as a separation device--in contrast to, say, degradation--lies in the fact that very large momentum changes are required in order that pions or protons have the same deflection as K mesons; for example, the spectrometer deflects equally pions with 0.33 Bev/c, K mesons with 1.17 Bev/c, and protons with 2.23 Bev/c. Thus the requirement on the initial momentum selection is extremely mild.

An elementary system utilizing a velocity spectrometer is shown in Fig. 2a. The lens produces at a distance  $q$  an image of size  $I$  of a target of size  $0$  located at a distance  $P$ . On the way to the lens the beam passes through a momentum analyzer  $M$ , which admits only a narrow momentum band to the lens, and on the way from lens to image the beam passes through the velocity spectrometer. The crucial quantity is evidently the ratio  $\eta$  of separation  $S$  to image size  $I$ :

$$\eta = \frac{S}{I} = \frac{\alpha P}{0} \left( 1 - \frac{\ell}{2q} \right). \quad (4)$$

The  $\eta$  could be increased by moving the lens to the other side of the spectrometer with a proportional decrease of the solid angle  $\omega$ . Equation (4) shows that to utilize the full potentialities of the spectrometer  $q$  should be much larger than  $\ell$ . However, this would result in a great loss of K mesons due to decay in flight. For this reason the system shown in Fig. 2b was adopted;  $q$  is now effectively infinite, hence Eq. (4) becomes

$$\eta = \frac{ap}{0} \quad (4a)$$

Further improvement of  $\eta$  can be achieved only at the expense of  $\omega \approx d/P$ . In fact, since  $a$  is inversely proportional to  $d$ , it is clear that  $\eta \omega$  can be improved only by increasing the product  $V \ell$  or decreasing the size of  $\theta$ .

Whether a system such as that proposed in Fig. 2b is, in fact, practical depends on (a) how much bigger the actual images produced by existing equipment are than those given by geometrical optics, and (b) how well one can prevent scattered pions from sneaking into the K image.

There are many causes that tend to extend the region where particles hit beyond the confines of the geometrical image. Among these, the most important are the chromatic and nonlinear aberrations of the focusing quadrupoles, the multiple scattering of the particles as they pass through the exit thin window of the accelerator, and the halo around the target due to decays of pions and strange particles. Incidentally, the aberrations of a two lens system are only slightly larger than those of a single lens.

It is difficult to make precise estimates of the effect of scattered particles, since this would require detailed calculations of the momentum and angular distributions from all conceivable sources of particles (target holder, etc.) or scatterers. Although it is possible to arrange the beam-defining stops so that very few particles can reach the K-meson image as a result of a single scattering, the number of particles available for scattering is so large compared with the expected K flux in the proper angular and momentum interval that protection against single scattering cannot be regarded as adequate.

For all these reasons it seemed desirable to stop the pions in an absorber and use the K-meson image as a source for another complete state of separation. This double separation is shown in Fig. 3.

In comparison with, say, simply doubling the length of the spectrometer, this arrangement offers several distinct advantages. The problem of scattered particles does not exist in the second stage in the same way as in the first stage: instead one must be concerned only about the possibility that the "out-of-focus" image of the first slit due to off-momentum scattered particles passing through it will overlap the second K-meson image. Such particles can be eliminated by a final bending magnet. The target halo naturally does not exist for the second stage. Finally, the vacuum system required for the spectrometer can be extended through the quadrupole lenses all the way from one slit to the other. Thus multiple scattering is eliminated as a source of undesired particles.

#### Detailed Consideration of the Apparatus

As framework for a detailed discussion, a sketch of the proposed beam is given in Fig. 4. The secondary particles resulting from the bombardment of a target in the Bevatron are momentum-analyzed by the Bevatron magnetic field. Those with a 1.17-Bev/c momentum move along the indicated trajectory, leave the Bevatron vacuum system through the thin window, and enter the system through a series of collimators placed in a magnetic shield. This shield is located in a large hole cut into the return legs of the Bevatron magnet. The magnetic shield prevents the inhomogeneous magnetic field in this hole from causing aberrations of the target image. The first quadrupole lens system then forms an essentially parallel beam for the spectrometer and the system continues as shown in Fig. 3, except that the fringe field of the final bending magnet is also used for vertical focusing of the beam.

The characteristics of the various components will next be discussed in detail.

#### Target

The location of the target is established by the requirement that 1.17-Bev/c particles emitted at 0 deg with respect to the proton beam pass through the center of the hole in the leg slab. Lawrence Radiation Laboratory has an IBM 650 Code (ETHELBERT) which computes particle trajectories in the median plane of the Bevatron, given the initial position, direction, and momentum of the particles. It can also perform a perturbation calculation to determine their vertical motion

once the orbit in the median plane is known. In Fig. 5 let  $T$  be the center of the target and  $A$  the center of the upstream end of the front collimator. The Bevatron fringe field is such that particles moving near the indicated central trajectory are focused horizontally and defocused vertically. The following derivatives given by ETHELBERT completely describe the focusing properties of the fringe field in the median plane:

$$\left. \frac{d\lambda}{dg} \right]_{P = 1.17 \text{ Bev/c}, S = 0} = 0.0130 \text{ radians/inch,} \quad (\text{A})$$

$$\left. P \frac{d\phi}{dP} \right]_{S = 0, \lambda = 0^\circ} = 0.3985 \text{ radians,} \quad (\text{B})$$

$$\left. \frac{d\phi}{d\lambda} \right]_{P = 1.17 \text{ Bev/c}, S = 0} = 0.0266, \quad (\text{C})$$

$$\left. \frac{d\phi}{dS} \right]_{P = 1.17 \text{ Bev/c}, \lambda = 0} = 0.0126 \text{ radians/inch.} \quad (\text{D})$$

As will appear in the section on beam optics, the horizontal aperture of the first quadrupole lens had to be limited to 5.5 in. in order to avoid large nonlinear aberrations. Thus Eq. (A) yields a horizontal angle  $\Delta\lambda$  accepted by the system equal to  $7.2 \times 10^{-2}$  radian. Equation (C) then shows that at a given momentum particles entering from a given point on the target differ by only  $9 \times 10^{-4}$  radian in direction; for purposes of the horizontal optics they may be regarded as parallel. Equation (B) gives the dispersion and (D) the horizontal angular size of the target.

The calculation of the vertical trajectories of the particles showed that although the actual target was 117 in. from point  $A$ , its virtual image due to the Bevatron fringe field was 79 in. from  $A$ . In addition, the effective position of the diverging lens was just at the thin window, 36 in. from  $A$ . Thus the effective solid angle is reduced by a factor of 0.55 if the virtual image is considered as the new source. The object principal plane of the first quadrupole lens was 184 in.

downstream from the virtual image. To prevent the beam from striking the spectrometer plates it was limited to a height of 2 in. at this plane by the second of the two collimators. As a result the vertical solid angle of the system was  $6.0 \times 10^{-3}$  radian. The total solid angle accepted by the system was thus  $4.3 \times 10^{-4}$  steradian.

The height of the target,  $0$  in Eq. (4) and (4a), is of course of crucial importance for the success of the separation scheme. In the direction of the beam, the thin window had a thickness of 165 mg of Al and hence an rms projected scattering angle of  $1.16 \times 10^{-3}$  radian. At the virtual target position this corresponds to an effective target height of 0.1 in. Since the actual target height is demagnified by a factor of 0.55, a 0.125-in.-high target increases the apparent target height due to multiple scattering by only 15%. Hence a 0.125-in.-high target was adopted.

Tests were run to establish whether a target of this height could be used without loss of beam. In these tests targets of various shapes made of plastic scintillator were mounted on a pinwheel target holder and viewed one by one by a photomultiplier as the beam struck. All targets were provided with a 0.125-in.-thick Lucite lip extending 0.125 in. radially. (When the lip was removed, the light yield dropped by 30%). Compared to large target which by hypothesis, collected 100% of the beam, targets 0.125 in. high and 0.50 and 0.25 in. along the radial direction collected 70% and 50% of the beam, respectively. The beam struck the target after the rf was shut off. The cause of the observed beam loss is not completely understood, nor is it known to what extent the yield may be affected by different beam steering. Nevertheless a radial dimension of 0.50 in. was selected for the target.

Two targets were chosen such that each could be flipped to the correct position in the Bevatron. One was aluminum, 5 in. in the beam direction, and the other tantalum, 3.3 in. long. On the basis of a geometric mean free path of the beam protons and the emitted K mesons, tantalum should give 1.3 times the K yield of aluminum. From a previous associated-production experiment,<sup>2</sup> the  $K^-/\pi^-$  ratio at the target was known to be  $0.007 \pm 0.003$  for  $0^0$  and polyethylene; from a previous antiproton experiment<sup>3</sup>, the forward 1.15-Bev/c pion flux from a 6-in.-long beryllium target was known to be in excess of  $3700$  pions/ $10^{10}$  protons/millisteradian/1%  $\Delta p/p$ . As is shown below, the momentum interval accepted

<sup>2</sup>Frank S. Crawford, Jr. (Lawrence Radiation Laboratory), private communication.

<sup>3</sup>Cork, Lambertson, Piccioni, and Wenzel, Phys. Rev. 107, 248 (1957).

by the system was 2.5%, and the length of the entire apparatus 1320 in. (so that only 1.9% of the  $K^-$  mesons emitted by the target survive). When all these factors, were combined, the minimum expected number of  $K^-$  mesons was  $0.33/10^{10}$  protons for the aluminum target. In terms of  $\epsilon$ , the desired  $\pi/K$  ratio in the chamber, the required suppression factor for the pions is  $7400/\epsilon$ .

The target holder, being much bulkier than the target, could be an important source of stray particles. To guard against this the target holder was attached by means of very thin supports so that the target holder proper was 1.25 in. below the target position and 2.75 in. radially inward. In the first spectrometer the pions were deflected upward so that the image of the target holder could not overlap the  $K$  image. In addition, two large clippers, one  $156^\circ$  and the other  $335^\circ$  in azimuth downstream from the target, prevented protons that had passed through the target from continuing around the machine and striking the target holder. The clippers were operated so that they would have reduced the beam hitting the target by a factor of 10 had they been plunged 1 in. deeper into the Bevatron aperture.

#### Spectrometers

A cross-sectional view of the velocity spectrometer is shown in Fig. 6. The coils are connected so as to generate a horizontal field; the walls A and B of the iron box serve as pole faces, E and F as return paths. The stainless steel plates C and D provide the coil form and are welded to plates A and B to complete the vacuum enclosure. The electrostatic deflection plates, 230 in. long, were made of 0.063-in. -thick stainless steel sheet 6-3/4 in. wide, and were spotwelded to 2-in. -diameter stainless steel pipe which also went around the ends. As a result of past experience with sparking it was decided to separate the plates 2.5 in. By electrolytic tank mapping it was found that when the plates were attached 0.125 in. below the tops of the pipes the field between the plates was constant to 1% to 4 in. from the centerline.

The uniformity of the electric and magnetic fields is, of course, crucial for the success of the separation scheme. At 1.17 Bev/c when the electric and magnetic forces on the  $K$  mesons cancel, they fail to cancel for pions by only 7.1%. In order to prevent the spectrometers from introducing significant aberrations the fields in the region used were held constant to better

than 1%. The magnetic field was found to be constant to 0.34%. On the other hand, maintaining the plate spacing constant to 0.025 in. proved troublesome. The natural tendency of the plates to warp is aggravated by (a) the necessity of keeping the number of supporting insulators as low as possible (in our case six, shown in Fig. 7), since each is a potential source of breakdowns, and by (b) the fact that each discharge corresponds to a sudden removal of a 20-kg load from each plate. At the time of installation the mean separations (averaged over the length of the plates) on the two sides of the plates differed by only 0.0006 in. At the end of the bake-out period the difference had increased to 0.009 in. Unfortunately it could not be ascertained what it was at the end of 3 months of operation.

Typically, the plates took about 3 to 4 days to bake out. This period was characterized by high steady drain and profuse sparking. When the potential refused to rise for perhaps a day, the plates were sanded with fine emery paper wherever they showed sparking damage, then cleaned thoroughly with acetone, then alcohol, and reinstalled. Each plate had its own Cockcroft-Walton rectifier--one positive, the other negative with respect to ground. The power transformers to the two rectifiers were connected so that the ripple voltages canceled. The sum of the two voltages, as metered by a resistive divider, was electronically regulated by controlling the input power. Since at high voltages resistive dividers are not very stable this method of regulation is not sufficiently reliable. An electrostatic sensing device would be preferable and the deflected pion beam is just such a device. As discussed in the section on beam tests the pion beam was used as final standard.

After the spectrometers had been in operation for some time the curve (given in Fig. 8) of spark rate of both spectrometers connected in parallel versus voltage was obtained. As a result of this information 380 kv was chosen as the potential between the plates. Towards the end of the run, a 24-hour period, chosen at random, shows a mean spark rate of 0.41 spark per minute, in agreement with Fig. 8. There was therefore no evidence of progressive deterioration (in spite of the fact that a few times air was accidentally admitted to the spectrometers due to forevacuum failures). This also implies that the

sparkling after bake-out caused no damage. Since the spark damage depends on the energy discharged in each spark it is evident that the energy stored in the gap and in the  $\sim 20$  feet of RG19 supply cable ( $\sim 15$  joules) was below the damage point. In a subsequent experiment when due to longer (SAMES) cables of larger capacity the stored energy was raised by a factor of 3, extensive damage to the plates due to sparking was encountered and water resistors had to be placed in series. The spark rate was independent of pressure in the range of  $10^{-4}$  to  $10^{-7}$  mm Hg.

The high-vacuum systems of the spectrometers were extended through the quadrupoles and terminated in 0.020-in. Al windows near the images, as shown in Fig. 4. At the upstream end, where because of the inaccessibility of the region the vacuum system was terminated very near the lens, a 0.006-in. Be window was used. A 0.002-in. Mylar bag filled with helium extended from there to the thin window of the Bevatron. The total multiple scattering due to the Mylar, helium, and beryllium amounted to  $3.5 \times 10^{-4}$  radian and increased the effective height of the virtual object to 0.148 in.

From Eq. (2) and the data of this section,  $a_{\pi}$  at 1.17 Bev/c is  $2.32 \times 10^{-3}$  radian. The magnetic field required in order that the K mesons satisfy Eq. (1) is 216 gauss.

### Beam Optics

Substituting the appropriate quantities into Eq. (4) gives  $\eta = 2.88$  if the target is taken to be 0.148 in. high and uniformly illuminated (rather than the actual multiple-scattering Gaussian distribution). This clearly does not leave much margin for poor focusing and aberrations. Therefore, the quadrupoles and the bending magnet were subjected to a careful study.

For these studies the usual wire-orbit method was used, but considerable effort was devoted to increasing its precision. Wherever the position of the wire had to be measured in space microscopes were mounted on a rectangular frame which could be moved in both directions perpendicular to the wire by means of screws. Wire-position measurements were then generally reproducible to 0.3 mm. Both because the optics of the beam required it and because it facilitated the treatment of the quadrupole as a thick lens in subsequent calculations, the wire was always sent into the focusing device parallel to the quadrupole axis. As a result focal points and principal planes were immediately established.

Each quadrupole lens consisted of three 8-in.-bore sections, the outside ones 16 in. long and the central one 32 in. The sections were spaced 9 in. apart. In order to avoid an excessive number of free parameters and also to have principal planes located symmetrically about the quadrupole, the two outside sections were operated at the same current. Figure 9 shows an example of the chromatic and nonlinear aberrations for such a lens system when it was adjusted so that the focal points coincided 152 in. from the center of the lens system. Both CDC (convergent, divergent, convergent) and DCD conditions are shown. The nonlinear aberration curve is that for the aberration which is of greatest interest for the beam geometry of this experiment: the variation of the focal length in the vertical plane for paraxial rays as they are displaced horizontally. As a result of such measurements the DCD condition was selected for the more critical vertical plane in spite of its greater chromatic aberration.

In order to facilitate quadrupole adjustments during the setup, maps were prepared relating the space of the center-section and end-section currents to the space of CDC and DCD image points. These maps were very useful when it was necessary during the tuning procedure to adjust the particle image in one plane while keeping the image in the other plane unchanged. However, in the end, the wire-orbit points were confirmed by particle images to a few inches.

Preliminary wire-orbit measurements on the final bending magnet (36 in. long, 18 in. wide, with a 4 in. gap and required to produce to  $30^\circ$  bend) showed that its focal length in the vertical plane varied by more than a factor of two when the rays were displaced laterally by 4 in. This was due in part to the fact that the constant field lines were not parallel to the edges and in part to nonuniformities of the field inside (at 19,500 gauss). It was found that this condition could be corrected by increasing the gap to 8 in. and placing shims along the side edges of the pole faces as shown in Fig. 10a; the field at the center of the magnet then varied from one side to the other as shown in Fig. 10b, and the image point in the vertical plane varied as shown in Fig. 10c. The abscissa in this case is the horizontal position where the wire crossed the center of the magnet. Evidently there now exists an 8-in. -wide region where the focal length varies by less than  $\pm 7.5\%$ . Since the aberrations of the second lens of a two-lens system are not as important as those of the first, this was satisfactory.

A sketch of the optical arrangement finally chosen is shown in Fig. 11. With regard to the horizontal plane it should be observed that the first quadrupole forms a real image of the target in the second quadrupole, and the final quadrupole forms an image of this image at the second slit. Because of the momentum dispersion due to the Bevatron field, images of different momenta appear along the H line in the second quadrupole. A collimator situated in this region can be used to define the momentum interval transmitted to the remainder of the apparatus. As a result of image-profile calculations to follow, this collimator was chosen to transmit a 2.5% momentum interval. With regard to the horizontal optics, the second quadrupole served merely as a field lens directing off-momentum particles back into the third quadrupole. At the second slit the horizontal image of the 0.5-in. -wide target was 3.7 in. The momentum dispersion at the second slit was 3.34 in./1%  $\Delta P/P$ , of which 2.32 in./1%  $\Delta P/P$  was due to the initial dispersion and 1.02 in./1%  $\Delta P/P$  due to the final bending magnet. Figure 12 shows plots of the momentum interval for any given point in the collimator in the second quadrupole and also at the second slit. The dotted regions are those cut off by the collimators. The momentum spread at a given point of the final slit is  $\pm 0.55\%$ . The entire image is 10 in. long at the second slit and is limited by the 8 -in. -wide slit to correspond to the 8-in. thin window of the bubble chamber.

It will be observed that within the velocity spectrometers the beam is slightly convergent in the vertical plane. In the second half of the system this

was dictated simply by the focal length of the shimmed bending magnet, but in the first leg the convergence was introduced deliberately so that off-momentum particles would not strike the spectrometer deflection plates. This is discussed more fully later. The vertical magnification of the first system was 0.88, that of the second, 1.68; the expected separation between the pion and  $K^-$  meson images was 0.336 in. for the first system, and 0.464 in. for the second.

Since the number of pions relative to the K mesons is so large, it was very important to have good estimates of the pion flux in the wings of the pion images. Image-profile calculations were carried out using the measured chromatic and nonlinear aberrations of the optical components and the sizes of the various apertures. Figure 13 shows the result of such a calculation for the second system, assuming a uniformly illuminated 0.2-in. -high first slit. It is clear that in spite of the aberrations the pion and K-meson images are well separated. In practice the first slit was not uniformly illuminated, hence the separation was actually better. As far as the first image is concerned it was found that the effect of plural scattering in the thin window was roughly equal to the effect of the aberrations.

#### Backgrounds

Thus far the discussion has dealt primarily with what one might call the "rational" beam. In addition one expects the presence of an "irrational" beam due to pions scattered from various surfaces, possibly emitted from sources other than the target, and possibly undergoing  $\pi \rightarrow \mu$  decay in flight. Because of the large number of particles that enter the channel and are available for scattering, estimates of the intensity of the "irrational" beam reaching the chamber are bound to be unreliable. Much effort was devoted to minimizing the "irrational" beam. However, as no serious calculations were made and during the experiment no time could be allotted to the determination of the efficiency of various collimation arrangements, it is quite possible that some of the precautions were unnecessary. A drawing showing the location of all the collimators is given in Fig. 14.

The following "philosophy" was used as a guide in the design of the collimation system. It was assumed that although the first separation system could not be very effective because of multiple scattering in the thin window, target halo, and scattering from beam defining collimators, all unavoidable in the first stage. In the second stage, on the other hand, these effects are not present. It seemed possible therefore to make the second stage essentially perfect. The aim was then to arrange the second separation in such a way that

a pion or muon coming through the first slit could not pass through the second, no matter what its momentum, barring  $\pi \rightarrow \mu$  decay or scattering from the vacuum chamber walls near the final bending magnet. The method for doing this is illustrated in Fig. 15. Let  $K$  and  $\pi$  be the  $K$ -meson and pion images at the proper beam momentum and let  $\pi'$  be the image of pions of some lower momentum  $P'$ . The dotted lines are the extreme trajectories of particles passing through the  $\pi'$  image. Clearly the lower trajectory just begins to pass through the  $K$  image. Hence scattered pions can get through the  $K$  slit only for momentum deviation  $\Delta P \geq |P' - P|$ . Now, if the dispersing action of the bending magnet is such that particles with  $\Delta P \geq |P' - P|$  are deflected beyond the lateral limits of the  $K$  slit, none can get through at all. This is suggested by Fig. 16b. The purpose of the vertical collimator in the third quadrupole was to limit  $\delta$  (Fig. 16a) for scattered particles.

In the present case, neglecting spherical aberrations and assuming a 0.1-in. -high first slit, one finds  $P'$  8.6% less than  $P$ , but it only 7.8% momentum change is required to displace the image laterally by the full 8-in. width. Thus the system would be completely opaque to pions. In practice it turned out to be necessary to enlarge the first slit to 0.2 in. to avoid large  $K$ -meson losses at the first slit. The corresponding  $P'$  value was 5% less than  $P$ , and hence a window ranging from 5% to 8% less than the beam momentum was opened up.

Although the second stage can be made opaque to pions and muons, at least in principle, there still remains the possibility that a pion coming through the first slit decays before reaching the second and the decay muon passes through the second slit. For a 0.32-in. -high second slit the probability of this is 0.6% to 0.9% per pion admitted through the first. It is therefore important to keep the number of pions transmitted through the first system small even if the second system is perfect. The same requirement applies in order that pion scattering in the second stage be negligible compared with the "rational" beam.

A rough calculation shows that, when pions hit 0.15 in. from the jaws of uranium slit,  $\sim 15\%$  enter the slit through the side because of multiple scattering (for muons this fraction would be considerably greater, since they do not suffer nuclear attenuation). Of the pions entering the first slit in this fashion, only  $\sim 1\%$  are within the solid angle accepted by the second separation stage. For particles entering the second slit through its side the probability of passing into the bubble chamber is  $\sim 5\%$ . Although these numbers are small, it seemed desirable to suppress such particles more efficiently. For this reason the slits

and also some of the critical collimators were made of Armco iron and magnetized so that negative particles passing through the iron would be deflected out of the beam. To reduce the power requirements and to avoid stray fields, side pieces were added in such a way that each slit formed a closed magnetic circuit. In Fig. 14 the dotted lines behind the slits and the iron collimators indicate the deflection of particles that have passed through the entire length of magnetic field. Uranium blocks were placed behind each of these magnetized devices to stop the deflected particles.

In the vertical plane the collimation system of the first stage consists of only one magnetized iron collimator placed at the entrance to the first quadrupole and backed up by a uranium catcher at the center of the lens. Since pions scattered from the upper face of this collimator could pass through the K image, the collimator faces were sloped to aim at the edges of the virtual target.

In the horizontal plane particles far removed from the beam momentum were eliminated by two iron collimators placed ahead of the first quadrupole. Since particles passing through the first iron collimator at a large angle could be deflected into the general beam direction by the magnetic field in the collimator iron, a uranium collimator was placed ahead of it to cover the critical region. A large amount of scattering due to off-momentum particles was expected from this collimator system. Therefore another collimator was placed ahead of the third quadrupole, where the second quadrupole forms an image of the front collimators. It was expected that a large fraction of these scattered particles, especially those in the critical momentum region near the beam momentum, could be removed in this fashion.

Finally, those particles whose momenta were close to the beam momentum were stopped in the momentum-defining collimator in the second quadrupole. In this connection it should be mentioned that the spectrometer is a very efficient collimator itself. If a particle has a momentum such that it leaves the spectrometer plates from the side then, upon leaving, it experiences the magnetic force without the bucking electric force. Hence it is deflected sharply upward and out of the beam before it hits the vacuum-chamber wall. The mild convergence of the beam between the plates was chosen so that pions would leave the plates on the sides before they collided with the upper plate regardless of their momentum. Since particles scattered from the upper plate could reach the K image, it was considered desirable to prevent such scattering.

As indicated in the section on spectrometers, the pions were deflected up in the first spectrometer so that the image of the target holder would not overlap the K image. In the second stage the pions were deflected down. This was based on the idea that those pions and muons which managed to get through the first slit iron would appear to enter the second stage from a source located somewhat above the first slit and would be imaged somewhat lower at the second slit. Then, if the pions were deflected upward, these stray particles might be imaged on the second slit.

#### Beam Tests

After the apparatus had been assembled and aligned by means of optical levels, and the vacuum systems had been put into operation the lenses were refocused, using pions. For these measurements a threefold scintillation-counter telescope was used, consisting of two large counters covering the entire beam, and one only 0.19 in. high. This last counter could be moved up and down to obtain beam profiles. The final profile at the first slit position is shown in Fig. 16; the counter size and the position of the expected K image are also indicated. When the counter size is unfolded from this profile a full width of 0.166 in. at half maximum is found. This image size should be compared with a full width of  $\sim 0.15$  in. obtained by folding the demagnified image of the multiple-scattering virtual source of 0.148 in. with the aberrations of the first stage. As indicated before, the second stage was designed to be opaque to pions for a 0.1-in. -high slit. However, this would have caused a 35% loss of K mesons; since a high K-meson yield seemed more important than complete pion suppression, a 0.200-in first slit was chosen. The nature of the particles far out in the wings of the distribution was investigated by an absorption experiment, which showed them to be pions and muons in a ratio of roughly 3:1. At the position of the K slit the flux is  $\sim 3\%$  of the value found at the pion peak, and presumably consists mostly of pions.

The image at the second slit had a full width at the half maximum of  $\sim 0.32$  in. as expected for a 0.2-in. source and a magnification of 1.68. Accordingly a 0.326-in. -high second slit was selected.

Next, the deflection sensitivities of the spectrometers were determined by observing the motion of the image out of the median plane when small currents were sent through the spectrometer coils with no potential applied to the plates. These were found to be 45 amp/in. and 32.5 amp/in. for the

first and second stage, respectively; these numbers are in agreement with the spectrometer excitation coefficient of 240 gauss in./amp and with the expected focal lengths of the second quadrupole and the bending magnet.

When the system is working properly the K mesons go through undeflected and the pions experience a small magnetic force. This force can be "mocked up" without the need for an electric field by putting appropriate small currents into the spectrometers. The relative particle flux obtained by counting behind the second slit as the two spectrometer currents were increased together is shown in Fig. 17. The dotted line was obtained by subtracting the counting rate obtained with a 12-in. Pb absorber between the counters and is thus primarily due to pions. Also shown in the figure are the potential between the plates corresponding to each current setting and the expected relative K flux at the second slit. Thus according to these measurements a 33% pion background and a 67% muon background were expected at 380 kv. The second stage therefore suppressed pions by a factor of 1000. The curve also shows that if the currents are increased by a small amount  $\Delta I$  beyond the point at which K mesons satisfy Eq (1), a considerable suppression of pions can be achieved at the expense of a slight loss of K mesons. For example, if both currents are increased by 1.50 amp, 30% of the K mesons are lost but the pion background is then only 11%. It should be mentioned that these measurements were carried out with a 0.19-in. -high counter, whereas the slit is 0.326 in. high. As a result the conclusions derived from these measurements were expected to be somewhat optimistic.

In order to steer the K mesons through the two slits the following method was employed. Sandwiches of three 0.19-in. -high scintillators were mounted so that each was viewed by an individual 1P21 photomultiplier. One such "triad" was mounted on ways in front of each slit such that the middle counter could be placed either in front of the slit or displaced above or below it by an easily measurable amount. The output currents of the photomultiplier charged capacitors whose potentials were displayed in succession on an oscillograph by means of a relay-actuated sampling device. A photograph of a typical oscillograph trace is shown in Fig. 18. (The sampling time of one of the capacitors was lengthened deliberately in order to avoid confusion between the two triads.) Now, in order to steer K mesons through the slits, the center "triad" counters were first placed in front of the slits, and the spectrometer currents required to steer pions through the system were noted. The spectrometer currents

were then increased by a factor of 1.0765, corresponding to the ratio of pion and K-meson velocities. At the same time the triads were displaced according to the known deflection sensitivities in such a way that the pions again struck the center triad counters. The apparatus was then tuned for K mesons and the triads served as a pulse-by-pulse monitor of proper steering. The system essentially amounts to using the pions as an electrostatic voltmeter.

It remains to discuss the results of measurements of the beam properties using the bubble chamber itself. Since curvature measurements on tracks are not sufficiently precise to give the beam momentum and its spread with the required accuracy,  $K_{\mu 2}$  decays in the chamber were used for this purpose. A decay muon, emitted backwards in the rest system of a 1.102-Bev/c K meson, has zero energy in the laboratory frame of reference. Thus from the angle of emission and the range of stopping decay muons very precise momentum measurements of the K mesons may be obtained. On the basis of 27 events of this character, the mean beam momentum at entry into the chamber is  $1.153 \pm 0.004$  Bev/c. This number should be compared with the design value of 1.173 Bev/c and a loss of 0.019 Bev/c due to the scintillation counters and the thin window, etc., in front of the chamber. When the errors of the measurements are unfolded from the observed momentum deviations from the mean, the remaining true momentum spread is  $\pm 1.5\%$ . No correlation between momentum and horizontal position in the chamber was found. This suggests that the horizontal aberrations, which were neglected in the design, were large enough to smear the horizontal image over a major portion of the (8-in. -wide) second slit.

The total K flux through the chamber was, of course, readily obtained by counting K decays and dividing by the well-known decay probability within the chamber (4.15%). Averaged over all kinds of operating conditions, the K flux during the experiment was  $0.87/10^{10}$  protons. This flux is roughly three times that expected. Since this greater yield is not accompanied by a better pion rejection than that predicted on the basis of Fig. 17, it appears likely that the pion-flux estimate used was too conservative. The K-meson yield from the Ta Target was  $\sim 20\%$  higher than that from the Al target. The pion contaminations from the two target materials were the same within errors.

The cross section for the production of  $\delta$  rays with energy  $E_{\delta} \geq 5.83$  Mev by a pion of  $\sim 1.1$  Bev/c is 28 mb, while that for K mesons is zero. Hence, when a track is observed which has a  $\delta$  ray with  $E_{\delta} \geq 5.83$  and then has a nuclear interaction, the track can be identified as being due to a pion. Then, by use of

the approximate cross section of 43 mb for the production of visible two-pronged pion events given by Baggett,<sup>4</sup> the total number of pions may be deduced. The pion contaminations are given in Table I for two operating conditions, (a) when both spectrometers were tuned to the K-meson peak and (b) when the current in the second spectrometer was increased, first by 3 amp and later by 2 amp beyond the K peak.

In addition to K mesons and pions, the beam contained a large number of muons, some satisfying all beam criteria, some of considerably lower momentum, etc. For the two operating conditions the analysis of all tracks in two typical rolls of film (about 350 pictures per roll) leads to the breakdowns given in Table II.

Table I

<u>Condition</u>	<u><math>\pi/K</math> Ratio</u>
$\Delta I_1 = 0 \quad \Delta I_2 = 0$	$50 \pm 18\%$
$\Delta I_1 = 0 \quad \Delta I_2 = 2 \text{ to } 3 \text{ amp}$	$8 \pm 11\%$

Table II

	<u>Numbers of tracks found</u>	
	<u>Conditions</u>	
	<u><math>\Delta I_1 = 0, \Delta I_2 = 0</math></u>	<u><math>\Delta I_1 = 0, \Delta I_2 = 2 \text{ to } 3 \text{ amp}</math></u>
Protons on target	$6.8 \times 10^{12}$	$7.8 \times 10^{12}$
Protons on target		
K Mesons (beam) $\pi$	534	596
Pions (beam)	202	35
Muons (beam)	731	625
All tracks	3722	3597
Beam tracks	1467	1256

For the design of future beams it is of considerable interest to understand how the pions found in the chamber managed to get there. The following remarks summarize the properties of the pion component:

- (a) The pions are all in a momentum band, ranging from 1.12 Bev/c to 0.75 Bev/c, with a relatively sharp upper edge.
- (b) Pions of all momenta are uniformly distributed in horizontal position in the chamber.
- (c) Pions tend to enter the chamber 1.5 cm higher than the K mesons.

An examination of Fig. 16 shows that some pions from the wings of the pion image are admitted to the second stage when the system is tuned to K mesons. Owing to chromatic aberrations these pions are likely to have deviations of about 2% from the central momentum (Fig. 12). Furthermore, the nonlinear and chromatic aberrations in the second quadrupole cancel for high momenta, but add for low momenta; hence the momentum for particles in the wings of the pion image is likely to be 2% low momentum. According to the discussion accompanying Fig. 15 such particles cannot come through the second slit. But that discussion did not include the nonlinear aberrations in the second system; if these are included such particles can just barely get through. This explains the sharp upper momentum edge of the pions. The lower-momentum pions are then those which passed through varying amounts of the collimator iron. They arrive high in the chamber because that is the only direction in which they can escape the magnetic field in the collimator. If this is the correct explanation for the pion component then the decision to deflect the pions downward in the second stage might have been an incorrect one. An examination of the vertical-plane optics of Fig. 11 shows (neglecting the slight convergence of the beam in the spectrometers and differences in focal lengths) that if an off-momentum particle manages, because of aberrations to get from the target to the first slit after being deflected upward in the first spectrometer, then, by symmetry, it will also pass through the second slit provided the spectrometer is arranged to deflect it down.

Figure 19 shows two bubble chamber photographs, one made when the separators were ~~tuned~~ to pions, the other when they were tuned to K mesons. As three K-meson decays appear in the second photograph it is obvious that the picture was not picked at random.

After the end of  $K^-$  experiment the beam was tuned up for antiprotons. At 380 kv the pions would have been deflected entirely into the plates, which would have made the triads useless and possibly would have increased the scattered-particle flux. For this reason the potential between the plates was reduced to 200 kv. The antiproton yield was then found to be  $0.5 \bar{p} / 10^{11}$ <sup>4</sup> protons, and the  $\bar{p}:\pi:\mu$  ratio with rather mild beam criteria was 33:7:60.

---

<sup>4</sup>Private communication from Dr. S. Goldhaber

Acknowledgments

It would be difficult to acknowledge the advice and assistance of all those whose aid was required during the design and construction of this beam.

First of all, we wish to thank Professor Luis W. Alvarez for his encouragement and support.

Bruce B. Cork and Dr. William A. Wenzel contributed invaluable advice concerning the construction and operation of the spectrometers.

Glen R. Lambertson advised us on the difficult magnetic shielding problem in the leg slab area.

The invaluable cooperation of Dr. Edward J. Lofgren and the Bevatron crews is gratefully acknowledged.

We wish to thank Lazarus G. Ratner and Joseph H. Dorst for their help during the extended wire-orbit and magnetic-field measurements.

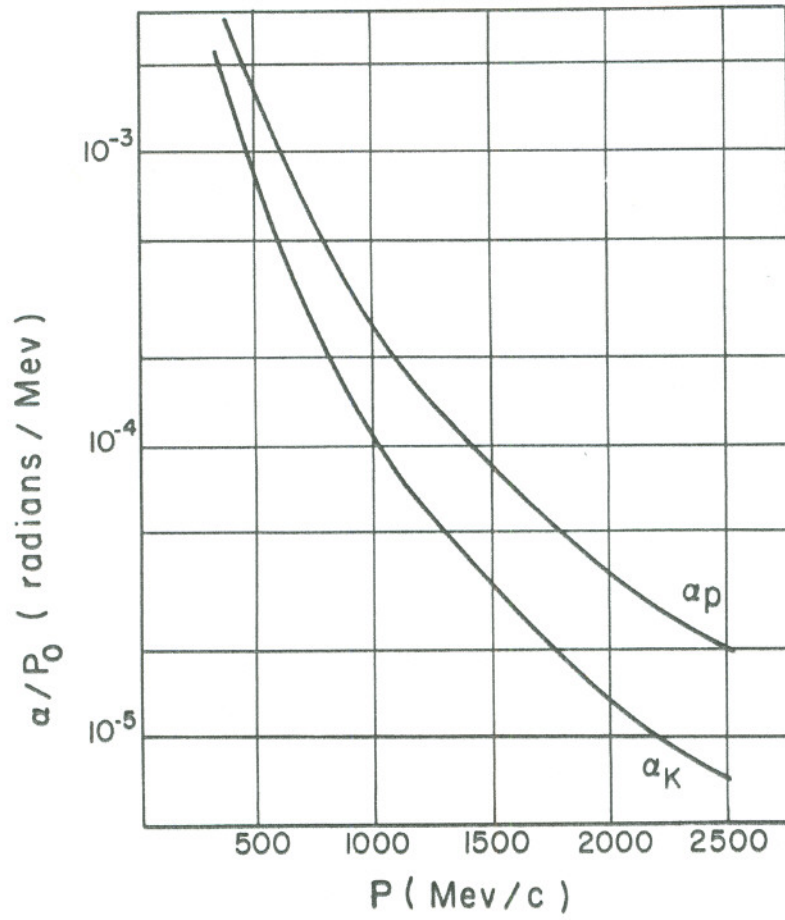
William W. Salsig and the Lawrence Radiation Laboratory engineering staff relieved us of all worries regarding mechanical design. In particular, George W. Edwards designed the complex vacuum extensions of the spectrometers.

The operation of the hydrogen bubble chamber was under the direction of James Donald Gow. The chamber crews, with Robert D. Watt and Glenn J. Eckman acting as crew chiefs, not only did a splendid job operating the chamber but also provided invaluable help with the high-voltage and vacuum systems of the spectrometers.

Last, but by no means least, we wish to acknowledge the assistance of William Graziano and Stanley G. Wojcicki. Without their tireless and conscientious help the project could not have succeeded.

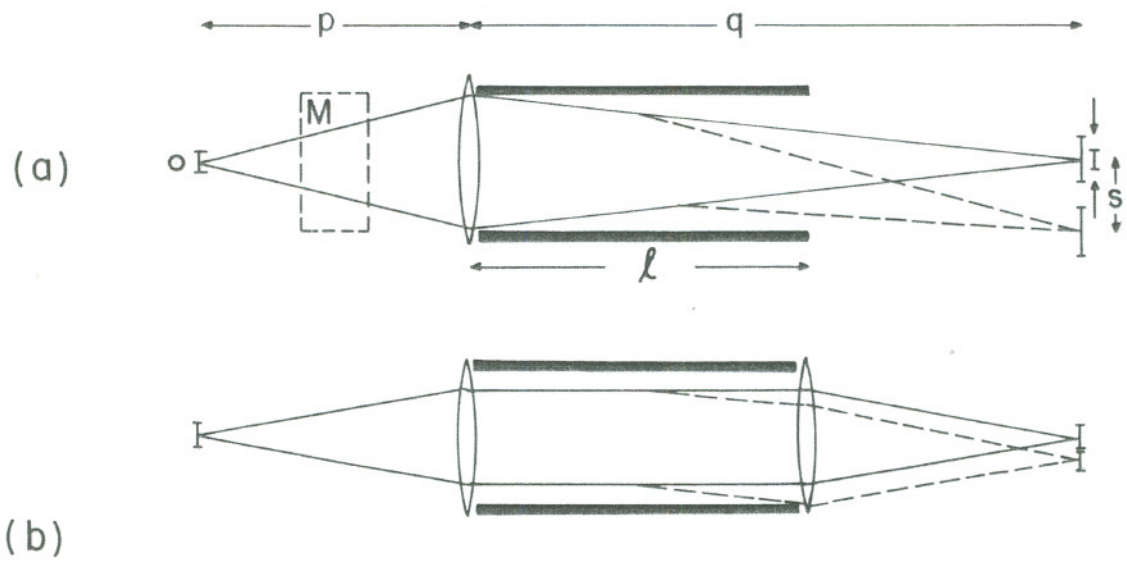
## LEGENDS

- Fig. 1. Angle of deflection  $\alpha_{\pi}$  of pions relative to K mesons, and  $\alpha_p$  of protons relative to K mesons versus momentum,  $P_0 = V\ell/d$ , where  $V$  is the potential across the plates in  $Mv$  and  $\ell$  and  $d$  are the plate length and separation, respectively.
- Fig. 2. Simple optical arrangements for use in connection with a velocity spectrometer.
- Fig. 3. Schematic arrangement for double separation system.
- Fig. 4. Complete layout of 1.17-Bev/c  $K^-$  beam.
- Fig. 5. Coordinate system for use in target area calculations.
- Fig. 6. Cross section through spectrometer.
- Fig. 7. Photograph of spectrometer plate assembly.
- Fig. 8. Spark-rate curve for two spectrometers.
- Fig. 9. Chromatic and nonlinear aberrations of 8-in. quadrupole lens triplet.
- Fig. 10. Nonlinear aberration of shimmed bending magnet.
- Fig. 11. Schematic optics of 1.17-Bev/c beam.
- Fig. 12. Dispersion plots at the first and second horizontal images.
- Fig. 13. Result of beam-profile calculation at the second slit position.
- Fig. 14. Arrangement of collimators for 1.17-Bev/c  $K^-$  beam.
- Fig. 15. Sketch to illustrate scheme for making second separation stage opaque to all pions.
- Fig. 16. Measured beam profile at the first slit position.
- Fig. 17. Measured pion attenuation of the entire apparatus.
- Fig. 18. Triad display pattern.
- Fig. 19. Bubble chamber photographs obtained when the spectrometers were tuned to pions and when they were tuned to  $K^-$  mesons.



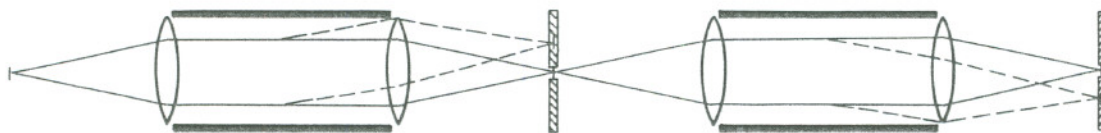
MU-18116

Fig. 1.



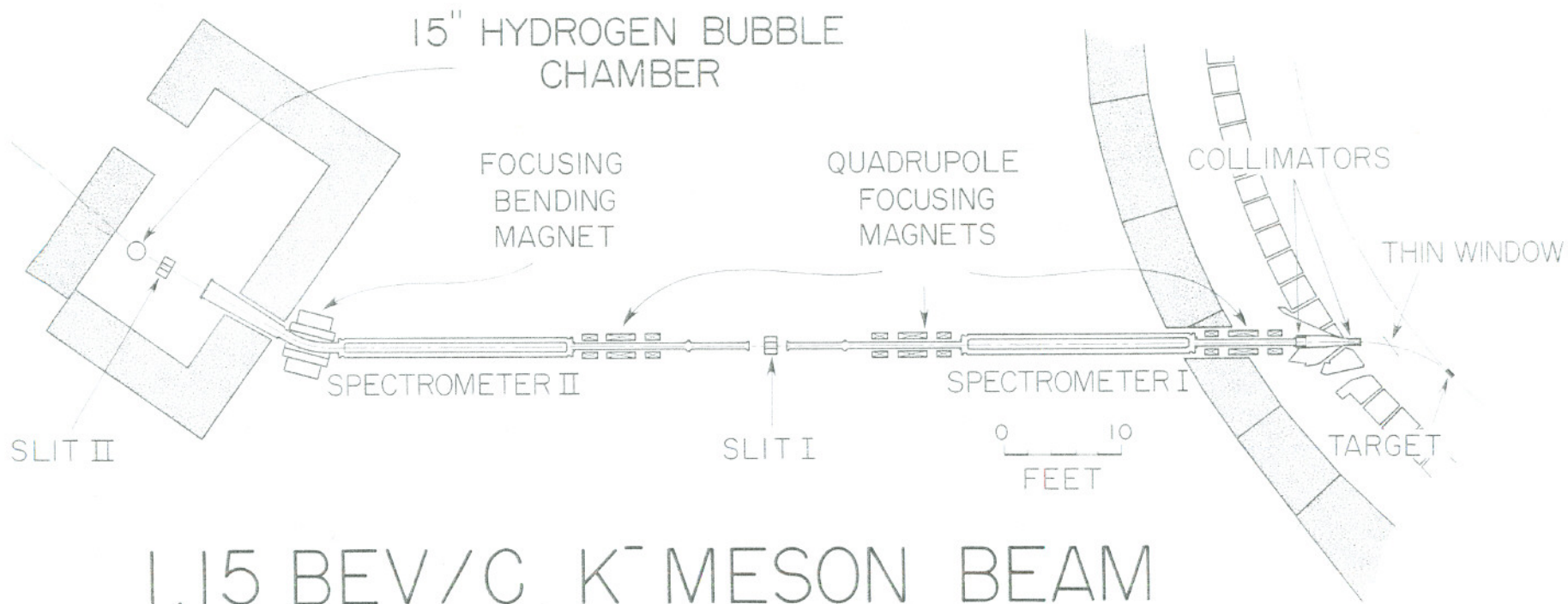
MU-18121

Fig. 2.



MU-18122

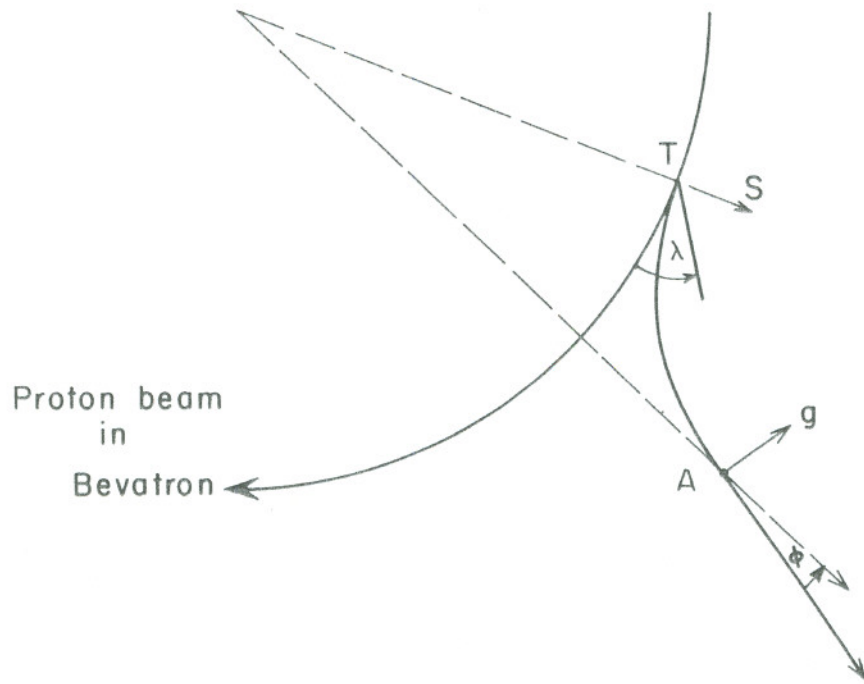
Fig. 3.



# 1.15 BEV/C $K^-$ MESON BEAM

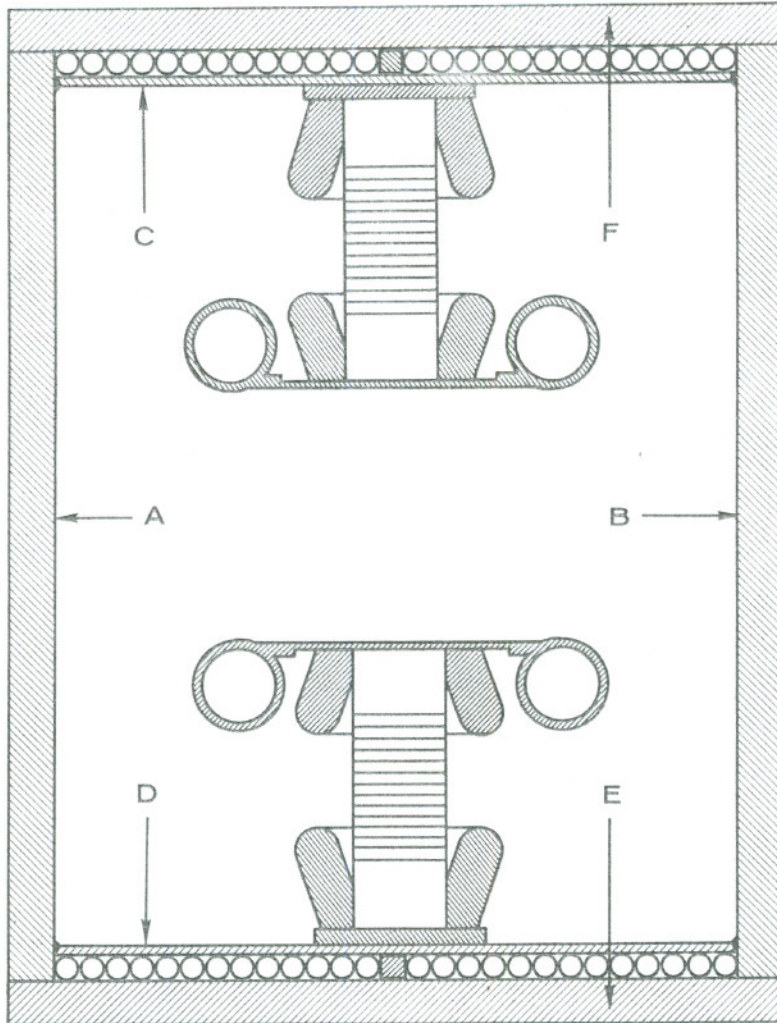
MUB-227

Fig. 4.



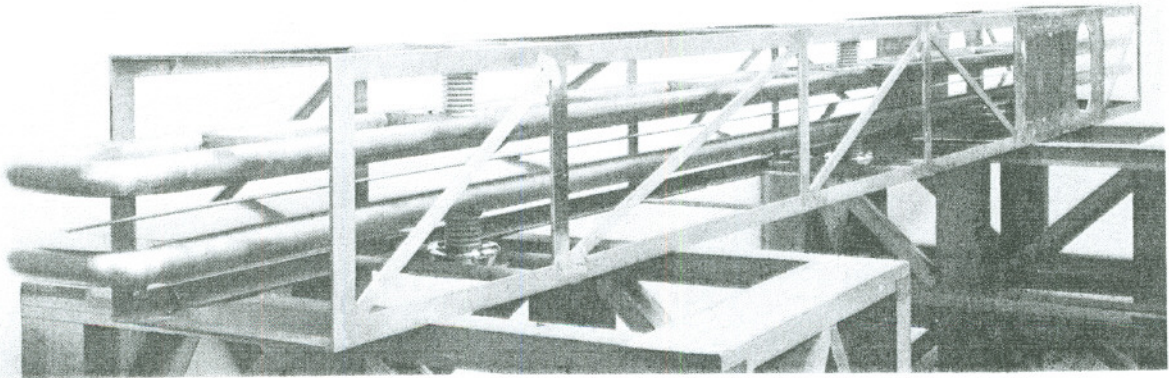
MU-18124

Fig. 5.



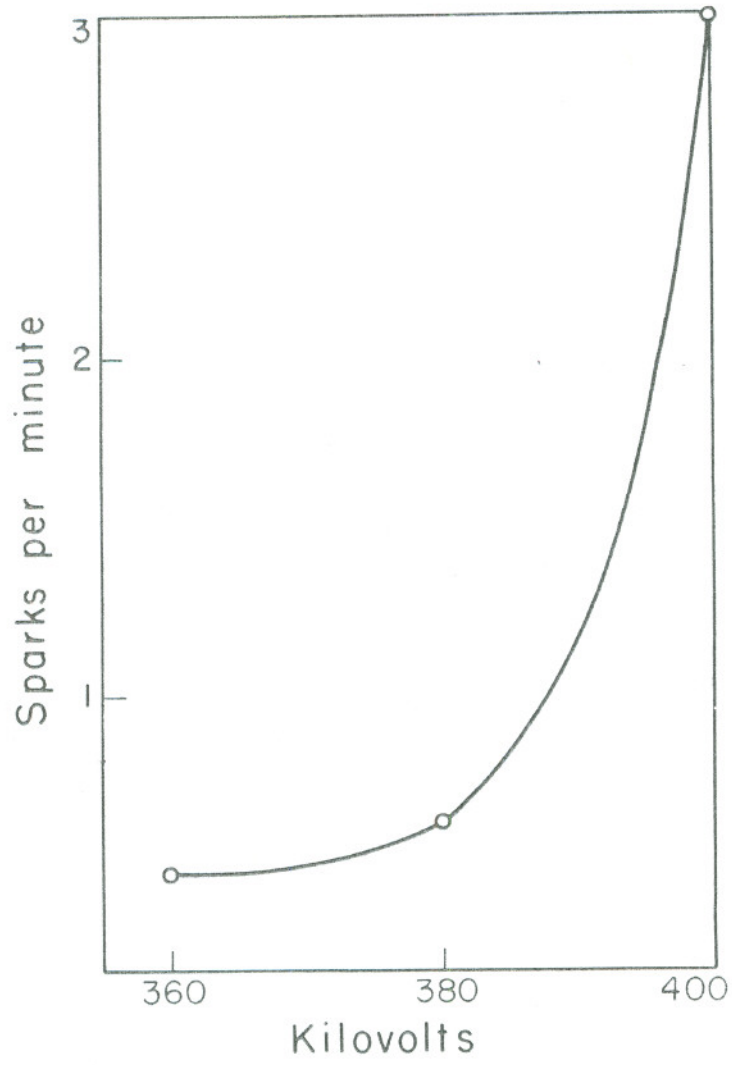
MU-18150

Fig. 6.



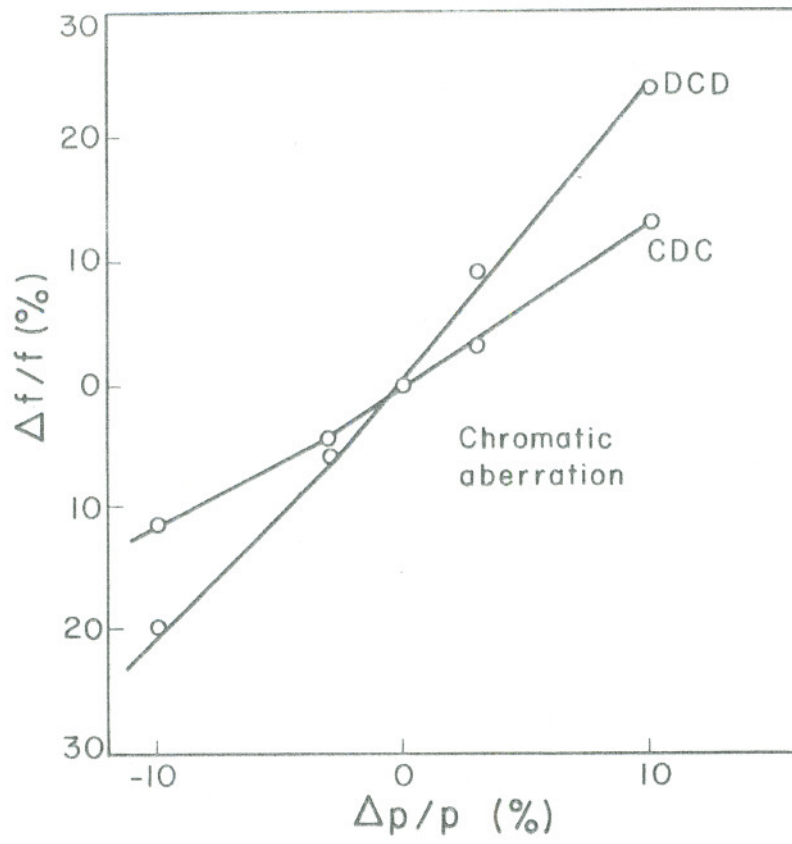
ZN-2223

Fig. 7.



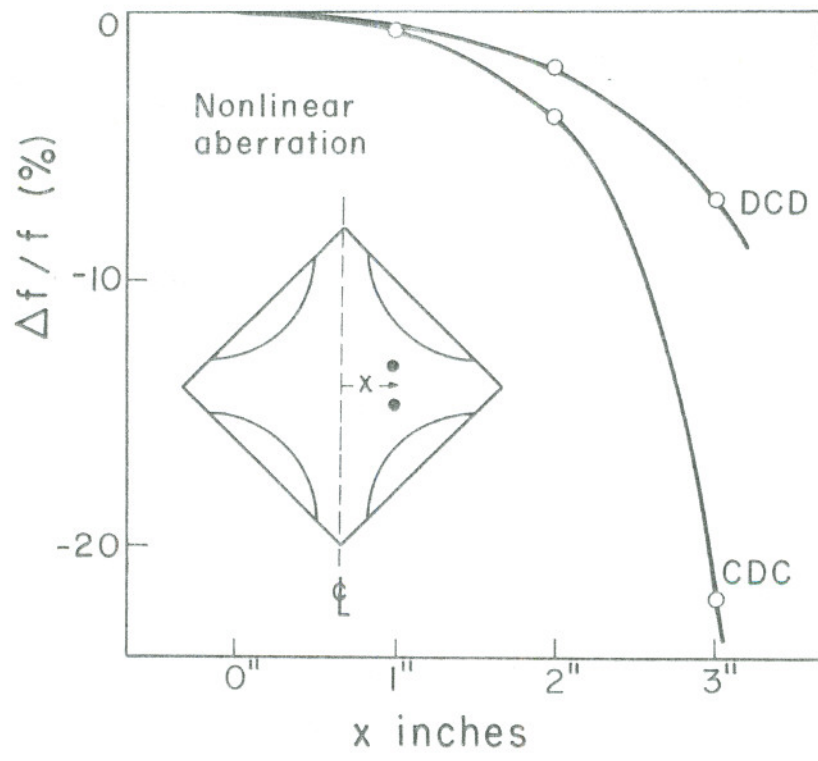
MU-18125

Fig. 8.



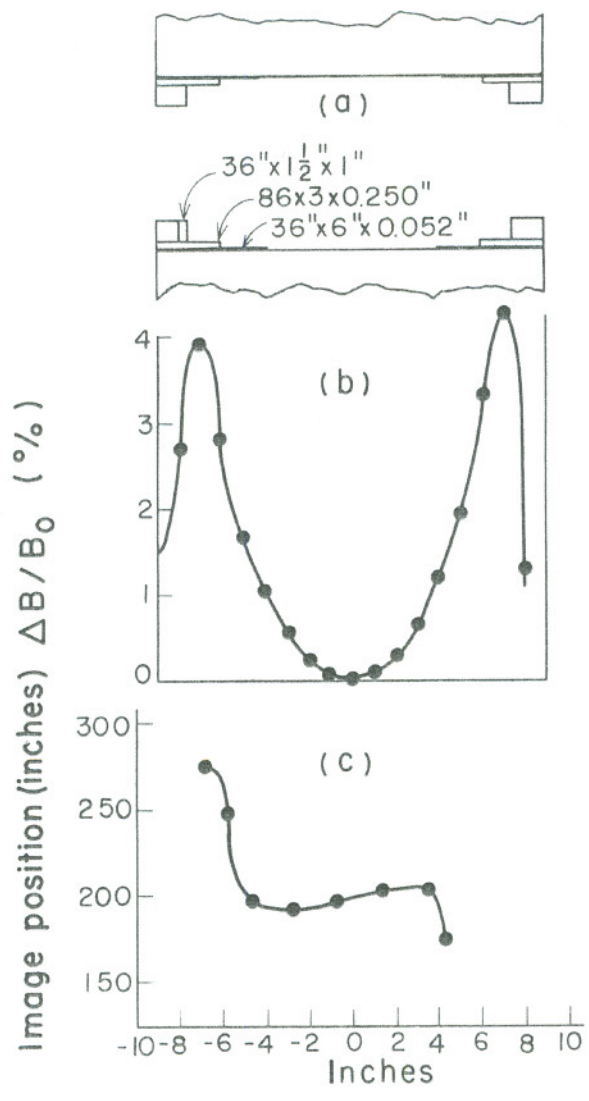
MU-18117

Fig. 9a



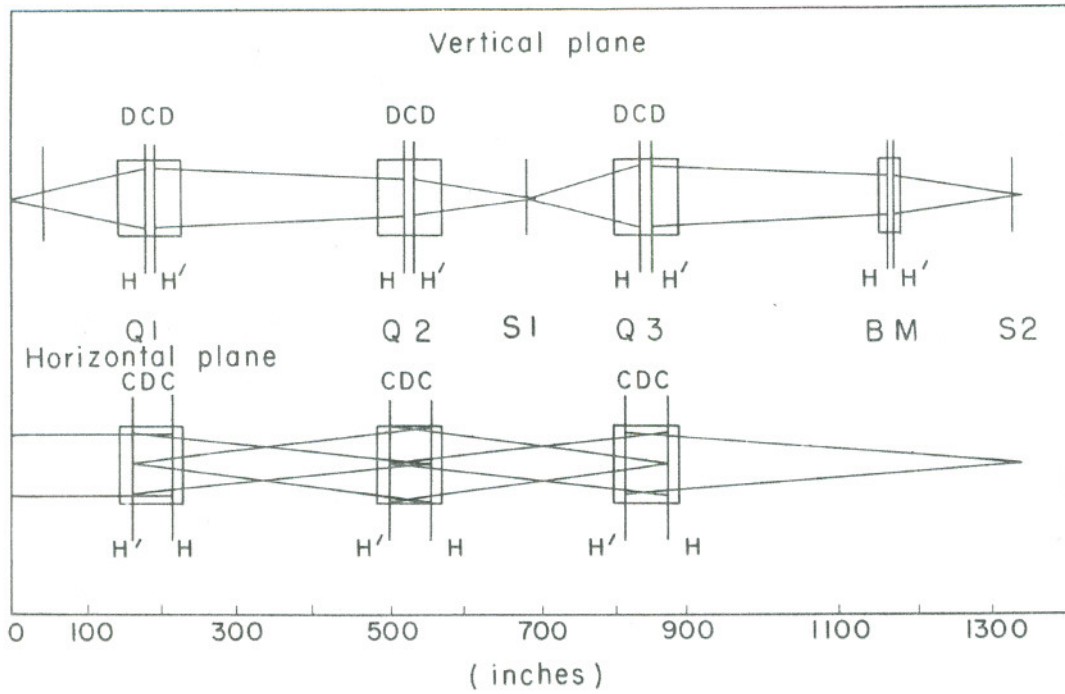
MU-18127

Fig. 9b



MU-18118

Fig. 10.



MU-18114

Fig. 11.

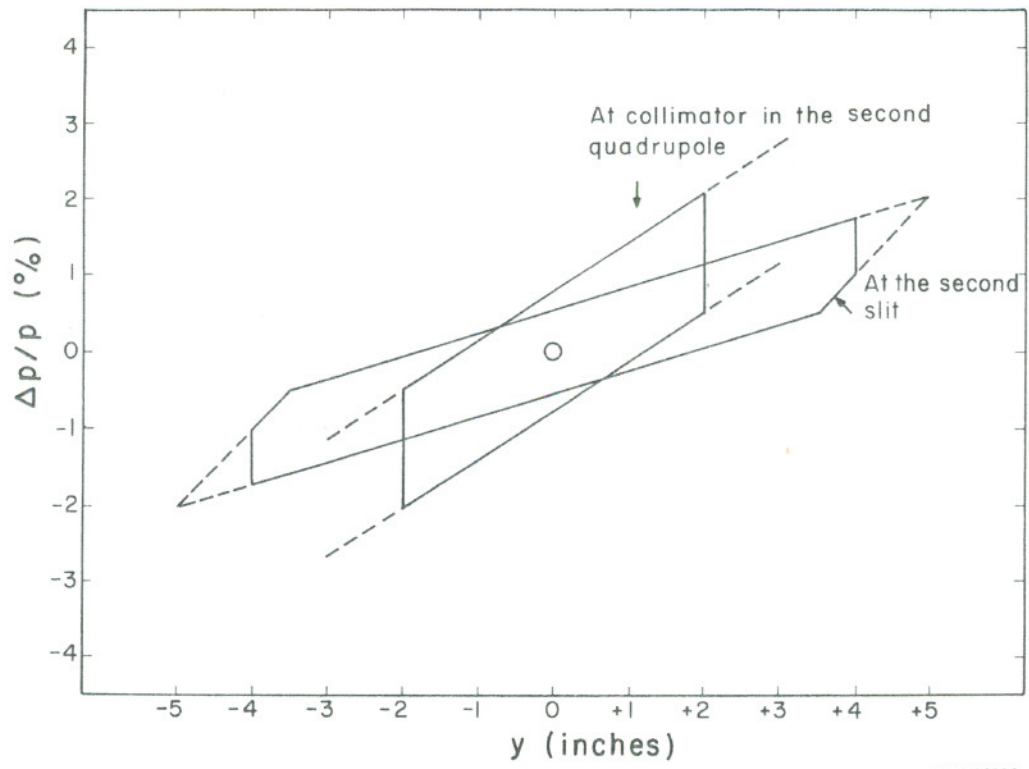
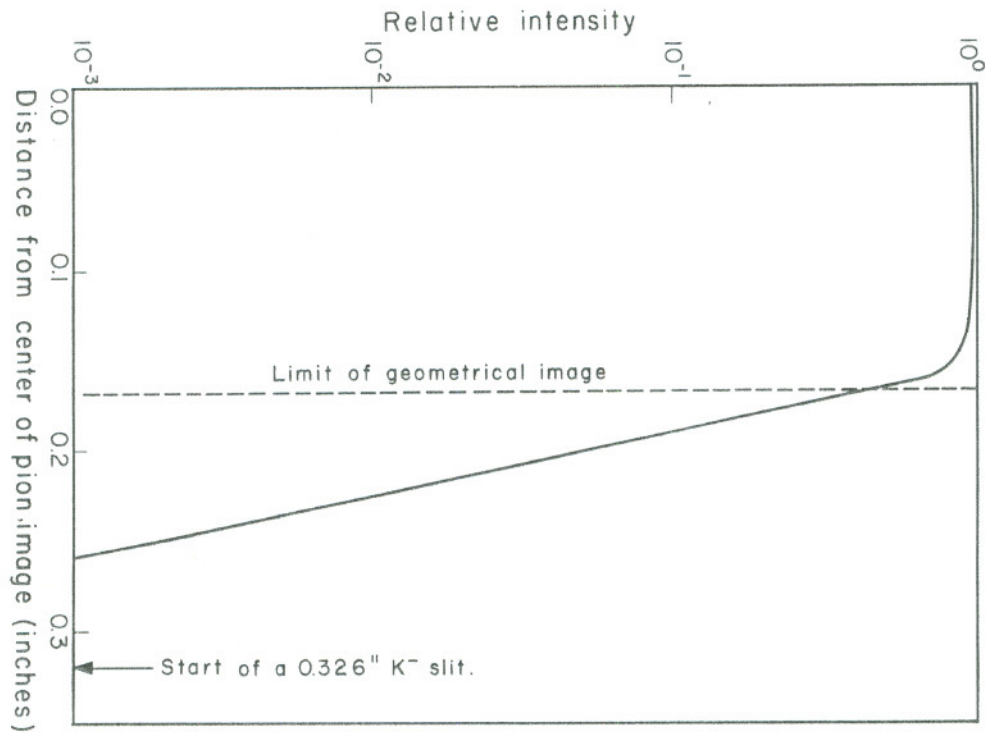


Fig. 12.



MU-18115

Fig. 13.

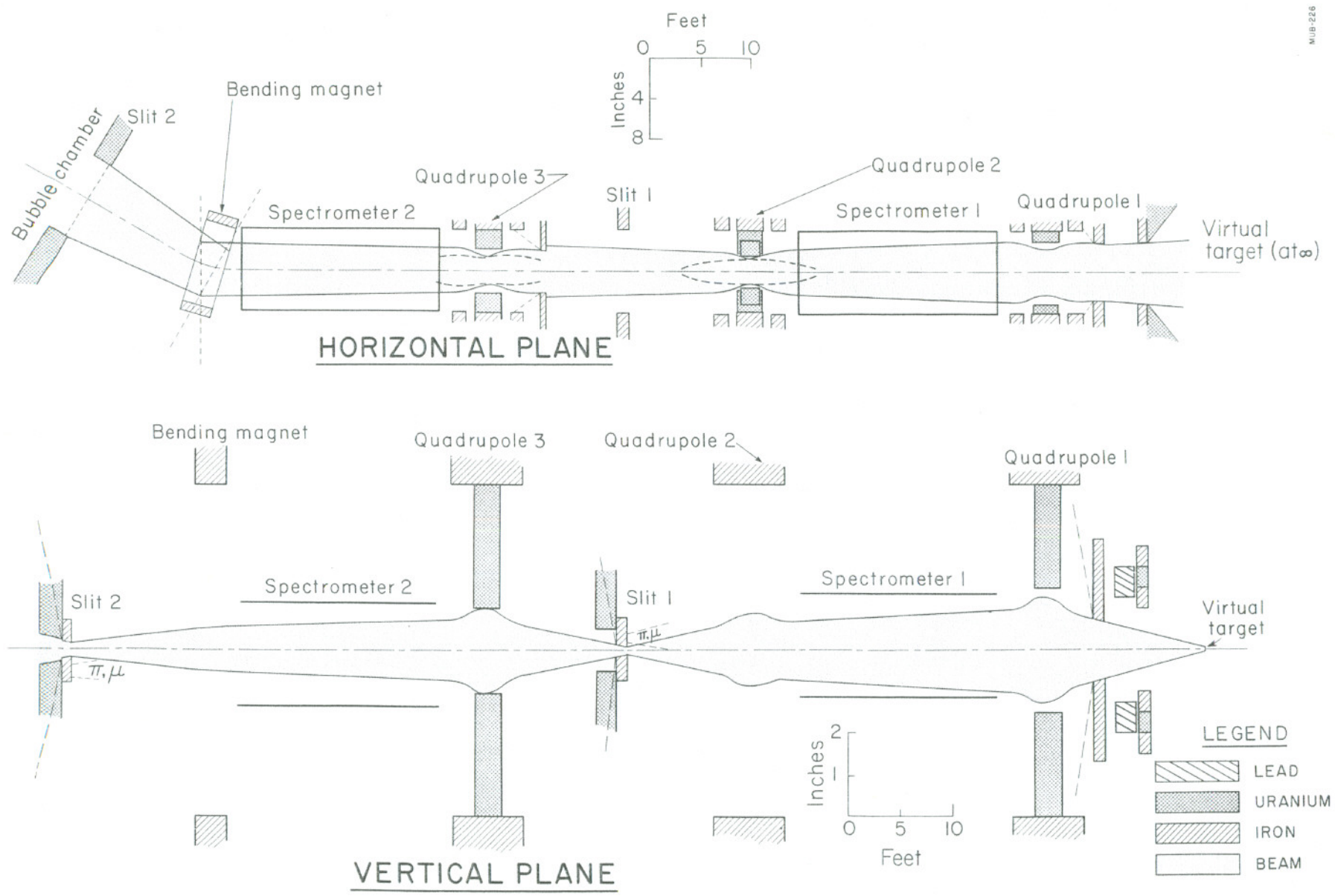
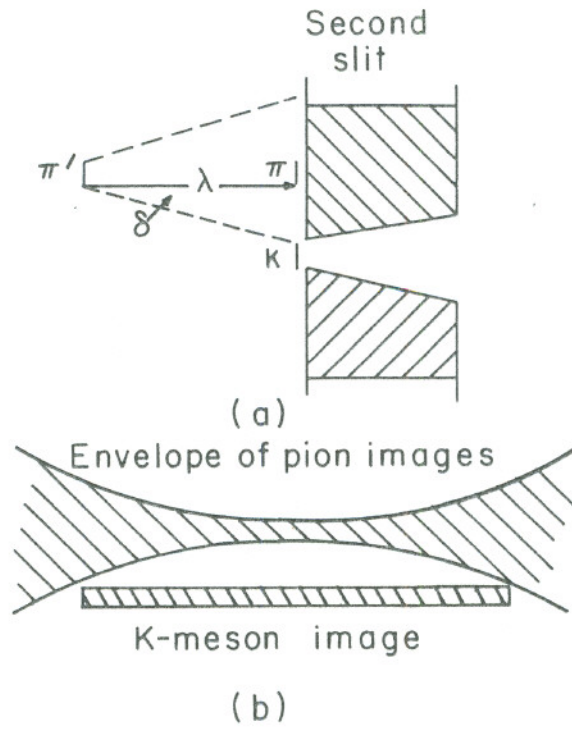


Fig. 14.



MU-18120

Fig. 15.

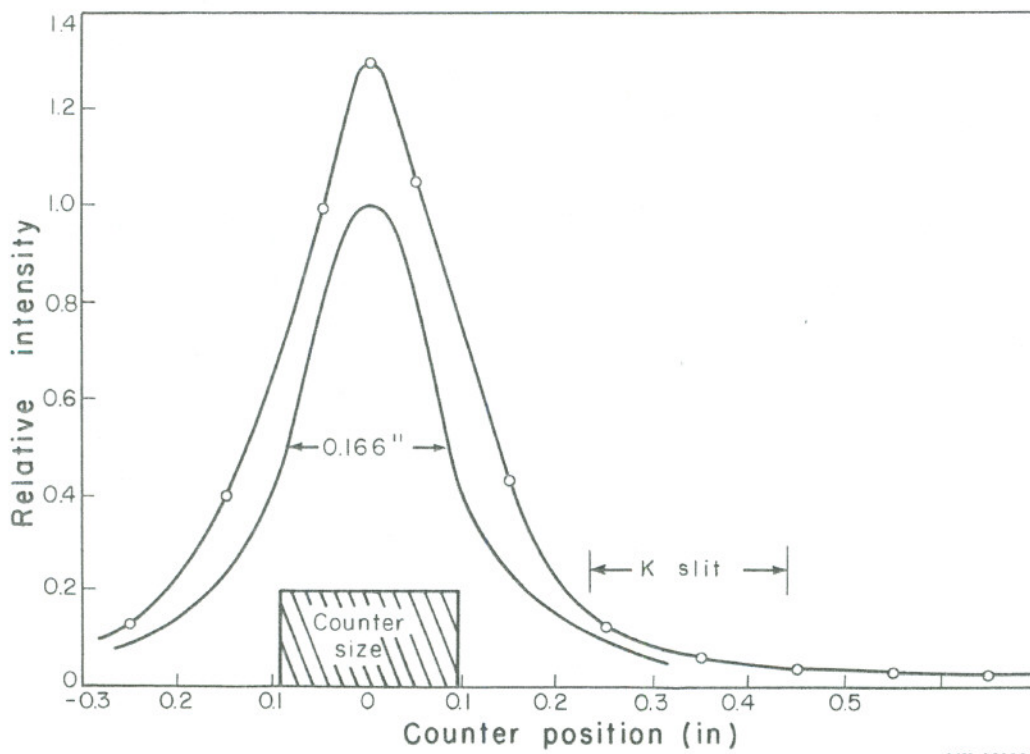
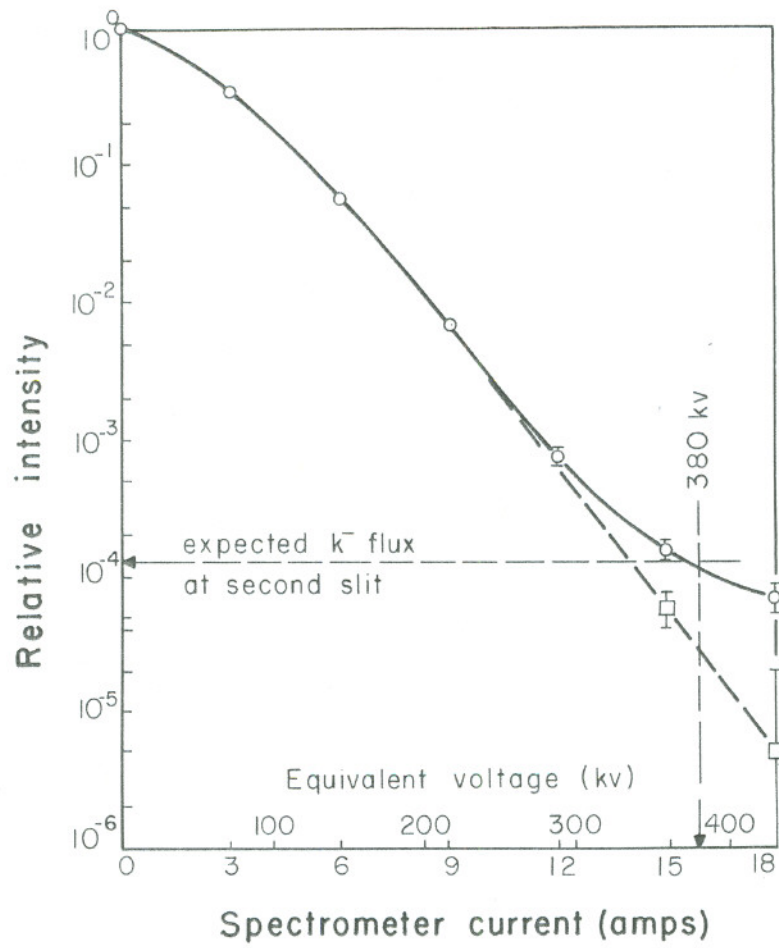
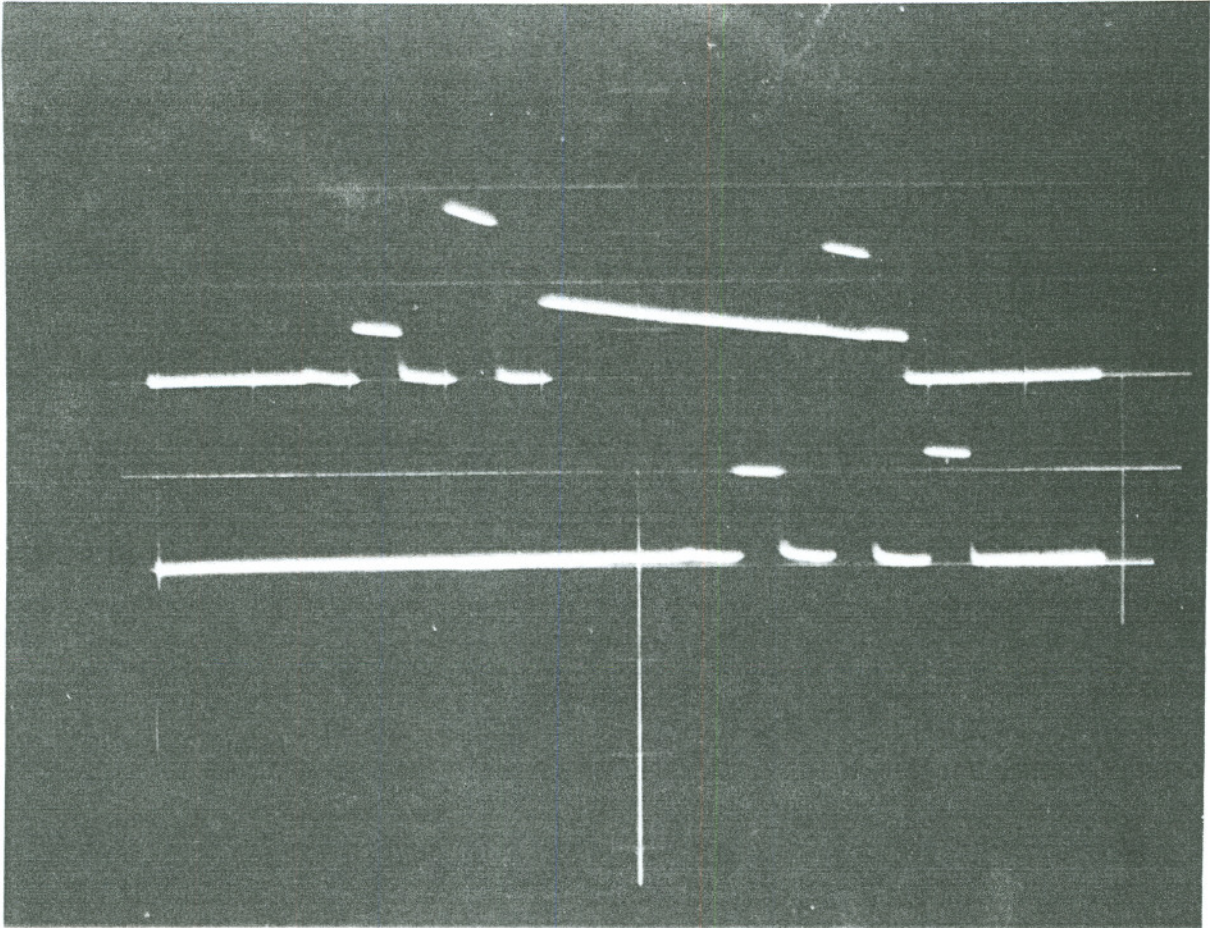


Fig. 16.



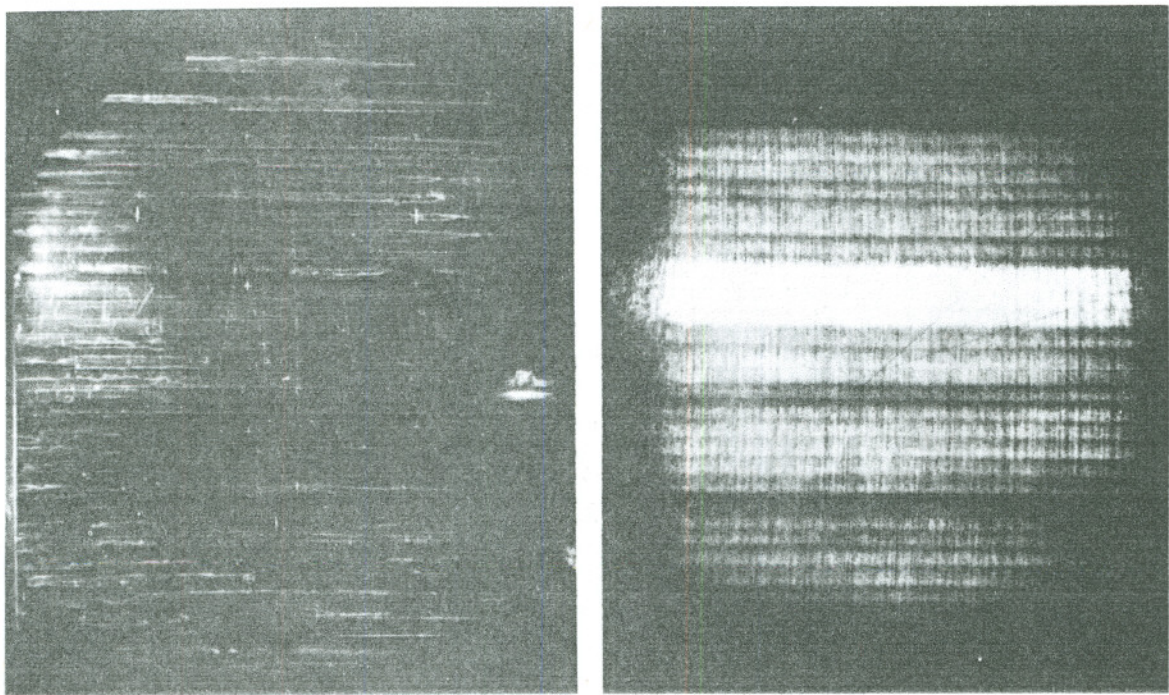
MU-18126

Fig. 17.



ZN-2224

Fig. 18.



ZN-2222

Fig. 19.